Biophysical Journal
Article

Biophysical Society

Chromatin Viscoelasticity Measured by Local Dynamic Analysis

Anat Vivante,[1,*] Irena Bronshtein,[1] and Yuval Garini[1]
[1]Physics Department and Nanotechnology Institute, Bar Ilan University, Ramat Gan, Israel

ABSTRACT The nucleus in eukaryotic cells is a crowded environment that consists of genetic code along the DNA, together with a condensed solution of proteins, RNA, and other molecules. It is subjected to highly dynamic processes, including cell division, transcription, and DNA repair. In addition, the genome in the nucleus is subjected to external forces applied by the cytoplasmic skeleton and neighboring cells, as well as to internal nuclear forces. These forces oppose the need to maintain the genome order, which may be compensated by the internal nuclear viscoelastic properties that can restrain these forces. The structural and mechanical properties of chromatin inside the nucleus are still not fully clear; however, their importance for the proper functioning of the cells is unquestionable. Different approaches have been developed for this aim, ranging from directly measuring the dynamic and elastic properties of chromatin to studying the interactions of chromatin with the surrounding envelope and nuclear bodies. Although the elasticity of naked DNA in vitro is well characterized, the elasticity of chromatin in live cells is more complex and is still not fully understood. Here, we studied the elastic properties of chromatin by dynamic measurements in live cells, followed by viscoelastic modeling. We measured the trajectories of single chromatin loci, centromeres, and telomeres in live cells and analyzed their dynamics using the Langevin formalism. We assumed that the overall effect of the chromatin network forces can be modeled for each locus by a local harmonic potential and calculated the effective force constant. In addition, we assumed that this harmonic force results from the chromatin network formed by the internal polymer structure together with cross-links formed by the protein complex. We show that lamin A has the greatest effect on chromatin viscoelasticity and that its removal leads to a significant reduction in the local harmonic force.

SIGNIFICANCE The structural and mechanical properties of chromatin inside the nucleus are still not fully clear; however, their importance for the proper functioning of cells is unquestionable. We study the elastic properties of chromatin by dynamic measurements of single loci in live cells, followed by viscoelastic modeling. More specifically, we analyzed their dynamics using the Langevin formalism. Importantly, we found that lamin A renders essential viscoelastic properties to the chromatin; however, this is completely modified in cells that lack lamin A. This indicates the importance of the protein as well as the viscoelastic properties of chromatin for proper cell functioning. Furthermore, the nucleus stiffness was shown to play an important role in preventing cancer metastasis by acting as an obstacle when the cell metastasizes through narrow capillaries.

INTRODUCTION

The organization of chromatin and the packing of DNA incorporates different scaling levels. Initially, the DNA itself is a rather rigid polymer with a persistence length of ~50 nm, which gives it a rather stiff character. At the next level, however, nucleosomes that are ~11 nm wide shorten the total length by a factor of ~6. Beyond that level, at the ~100 kbp range, HiC data were used to explore the existence of topologically associated domains, which have a typical size of ~200–500 nm (1). These mechanisms result in the formation of chromosome territories that are well maintained in the nuclear volume. Furthermore, in previous work, we have shown the existence of chromatin cross-links that form a higher order of chromatin on a scale of 0.5–2 μm (2).

The nucleus envelope is coated from the inner side by lamina. The lamina is composed of intermediate filament proteins, mainly lamin A and C (alternatively spliced products of a single gene, LMNA), together with lamin B1 and B2, which are the products of two additional genes, LMNB1 and LMNB2. The lamin proteins form dimers by

Submitted October 1, 2019, and accepted for publication April 1, 2020.

*Correspondence: anat.vivante@live.biu.ac.il

Editor: Gijs Wuite.
https://doi.org/10.1016/j.bpj.2020.04.002

the coiled-coil formation of their central rod domains, and the dimers assemble head to tail into polar polymers (3). They bind to the chromatin through their α-helical rod-like domains and form lamina-associated domains (4). Fluorescence recovery after photobleaching analyses indicated that the assembly of lamins in the lamina results in stable structures (5). The lamins incorporated into the lamina have little or no mobility; however, a fraction of the nucleoplasmic lamin is mobile (6), and it was found to play an important role in the entire nuclear volume by cross-linking chromatin, as mentioned above.

Because the lamina can also bind chromatin, it provides another level of chromatin stability to the nucleus. All these mechanisms, each in its scale, provide the nucleus with its structural and dynamic properties, which are essential for the proper function of nuclear processes such as replication, transcription, DNA repair, and gene regulation.

The nuclear membrane and lamina are assumed to play an important role in resisting mechanical forces applied to chromatin. However, the involvement of chromatin itself in mechanical resistance has also recently been suggested (7) and measured (8). The nuclear elasticity was measured and found to be related to the chromatin condensation level; it was suggested that the elasticity results from two spring-like contributions of both the lamina and nuclear envelope as well as the chromatin condensation itself. The elasticity character of the chromatin was shown to affect the efficiency of the nucleus packing (9,10), and it is related to the regulation of genome architecture and nuclear programs (11).

The packing of naked DNA is best described by a polymer model. The DNA is known to be a semiflexible polymer that can be accurately described by the worm-like chain model and approximated by the freely jointed chain model (12). For a given polymer length, the two models have the same mean-square end-to-end distance. However, in the freely jointed chain, the polymer is modeled to have N freely jointed effective stiff rods, each with a Kuhn length, whereas the worm-like chain model assumes a continuously flexible rod with a characteristic persistence length that defines the bending stiffness of the polymer and equals half of the Kuhn length. These models have been well studied, and the flexibility of double-stranded DNA fiber is characterized by its $\sim$50 nm persistence length (13,14) and $\sim$2 nm for single-stranded DNA (15), as verified by using a DNA origami structure. One normally defines persistence length as a measure of the scale in which the direction of the polymer changes significantly along the polymer. It is common to describe the chromatin in the nucleus as resembling the Rouse chain model (16); however, the nucleus is more complex because it is expected to have cross-links as mentioned above, and the system itself is an active gel, two factors that are not considered in the classical Rouse model (17).

Much less work has been devoted to measuring the chromatin elastic properties. Cui and Bustamante measured the persistence length of a single chromatin fiber and found a persistence length of $\sim$30 nm (18). Dekker et al. used the 3C technique to estimate that the persistence length of chromosome in yeast is 28 nm (19), and further works enabled the development of more realistic polymer models (20). Bloom showed that the spring constant of naked DNA or chromatin is proportional to k_BT/l_p, where l_p is the persistence length and the spring constant is estimated to be in the order of fN/μm (femto-Newton per micrometer) (21).

Previous work in our lab examined the dynamic properties of chromatin to shed light on its organization and functions. We followed the diffusion of different chromatin loci in live cells and analyzed the volume of motion and the type of diffusion (2,22,23). We mainly measured the dynamics of telomeres and centromeres that are spread in the whole nuclear volume. In normal cells, we found that the dynamics of all chromatin loci are highly localized, and the volume scanned by each loci was $\sim$0.02 μm^3, which is very small compared to the nuclear size ($\sim 10^4$ μm^3). The diffusion was found to be anomalous and viscoelastic, which is in agreement with fractional or Langevin dynamics (24,25). However, the analysis was limited to characterizing the diffusion, without testing the data according to physical models for viscoelasticity.

We noted that many of the measured telomeres and centromeres were located in the inner part of the nucleus, 3–10 μm away from the nuclear envelope and lamina (2). Therefore, the constrained dynamics cannot be explained only by the effect of the lamina, and a local mechanism should be involved. Furthermore, we found that the strong localized dynamics is highly dependent on the presence of lamin proteins, especially lamin A, and that its depletion leads to unconstrained motion of all chromatin loci (2).

Here, we attempted to examine the mechanical properties of chromatin in live cells by analyzing the dynamics of single chromatin loci and using first-order approximation of an elastic model in the framework of the Langevin equation, which is adequate for the overdamped stochastic dynamics in the vicinity of a potential well. This model assumes that the dynamics of each chromatin locus is governed by its local diffusion coefficient and harmonic force constant, a version of a mean-field approximation that approximates the complex interactions as a single harmonic-like potential at every locus site. Although the nuclear environment is quite complex, as described above, most of the chromatin domains remain constrained in their local environment; therefore, they can be modeled as diffusing particles in an external potential well. Even if the potential is more complex, to the first order, the force can be modeled as linear with the particle distance from its central coordinate (Fig. 1).

We hypothesize that the constrained dynamics in the entire nuclear volume results from a stiff harmonic potential that originates from bonds formed by lamin A.

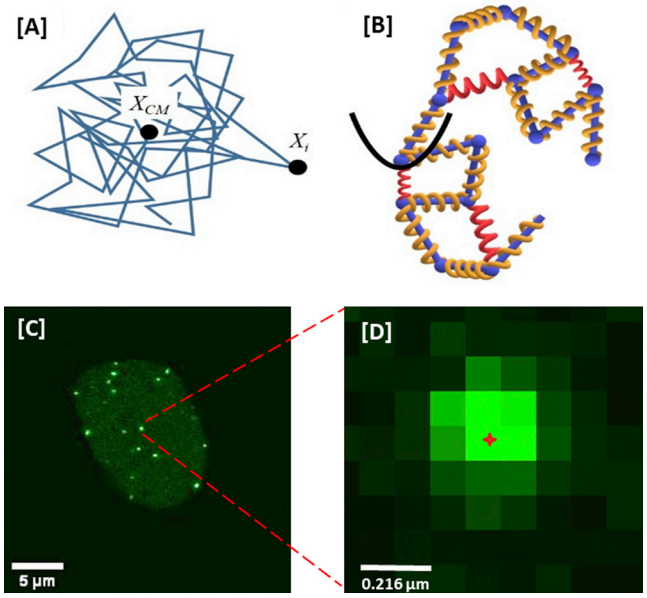

FIGURE 1 Chromatin dynamics model. (*A*) The trajectory of a single locus analyzed as the stochastic diffusion in a harmonic potential well around the center of mass is shown. (*B*) A simplified scheme of the viscoelastic model is given. The chromatin acts like a polymer, in which each site interacts with its neighbors through a given potential (*orange springs*) as well as having long-distance interactions along the chain due to cross-links (*red springs*). The overall effect is modeled as a local harmonic potential at each locus. (*C*) A fluorescence image of a typical nucleus expressing GFP-TRF1 proteins marking telomeres (*green*) is given. (*D*) A zoom-in image of one telomere shows an example of the spot size that was measured. The center of gravity (intensity) is denoted in red. The voxel size is 108 × 108 × 350 nm^3. To see this figure in color, go online.

Previous work performed by Amitai et al. (26,27) theoretically tested the validity of such a model for chromatin in the nucleus and found it to be adequate for a few different polymer models, including the Rouse chain. It was also tested experimentally for chromatin in yeast cells and further developed theoretically (28).

Using this model will allow us to estimate the effective local spring constant of chromatin and determine the effect that lamin A and other proteins have on it. Lamin A emerged in a previous work as an important nuclear organization protein (29).

The elasticity of chromatin is of great interest in a broad range of physical and biological systems. However, most previous work deals with theoretical estimation or simulations. Application of polymer model theories to live-cell dynamic measurements has only been preliminarily studied before in yeast cells, although it holds great potential for advancing our understanding of the elastic properties and cell function in general (26,30).

MATERIALS AND METHODS

We performed dynamic measurements of multiple chromatin loci in the nucleus by labeling the telomeres and centromeres of the chromosomes. We used mouse embryonic fibroblasts (MEFs) and human U2OS osteosarcoma cells. MEFs lacking lamin A/C (Lmna−/− MEFs) and their wild-type (WT) (LmNa+/+ MEFs) were kindly given to us by Prof. Susana Gonzalo from Washington University School of Medicine, St Louis, MO.

The MEF cells were maintained in Dulbecco's high-glucose modified Eagle's medium (Biological Industries, Beit HaEmek, Israel) containing 10% fetal bovine serum (Biological Industries), 1% penicillin and streptomycin antibiotics (Biological Industries), and 1% L-glutamine (Biological Industries). The U2OS cells were maintained in Dulbecco's low-glucose modified Eagle's medium (Biological Industries) containing 10% bovine serum and 1% penicillin and streptomycin antibiotics (Biological Industries).

For telomere tracking, we used transient labeling of the shelterin subunit TRF1 fused to green fluorescent protein (GFP) or red fluorescent protein (dsRed); for centromere tracking, we used the transient labeling of CENPA fused to GFP. The imaging system includes an inverted Olympus IX-81 fluorescence microscope coupled to an FV-1000 confocal set-up (Olympus, Tokyo, Japan), and a UPLSAPO ×60 objective lens with numerical aperture (NA) = 1.35. The cells were placed in a 37°C incubator (Tokai, Shizuoka-ken, Japan) with a 5% CO_2 level. The measurements were performed in three dimensions to correct for cell motion, as well as linear and rotational drift, although the actual dynamic analysis was performed only on the planar *xy* motion.

The nucleus drift and rotation were corrected according to the center of gravity of the species followed. We normally see about ∼50 telomeres in the nucleus, and because their motion is rather small compared with the size of the nucleus, the location of the center of gravity is an excellent means of calculating the center of the nucleus and the drift, if any exists. We therefore calculate the center of gravity at each time point and subtract it from the trajectory of each telomere position. For eliminating possible rotation of the whole nucleus, we consider only the rotation around the *z* axis and calculate the rotation angle in between each two projections of three-dimensional consecutive images after drift correction. The rotation matrix is calculated, and the coordinates of each telomere are multiplied by the inverse matrix. A set of 35 equally spaced planes of the cell nucleus were measured every 20.5 s with a voxel size of 108 × 108 × 350 nm^3.

The confocal microscopy allows a temporal resolution of 100 frames per second for two-dimensional images or ∼20 s per frame for three-dimensional images and for a spatial resolution in the range of 180 nm. However, single-particle tracking (SPT) provides a precision of ∼10 nm for finding the center position of each spot (Fig. 1 *D*; (31)). This value should not be confused with the resolution limit, which depends on the point spread function. For a confocal microscope, the diffraction-limited lateral *xy* resolution is roughly $s = 0.61\lambda/\sqrt{2}NA$, where λ is the emission wavelength and *NA* is the numerical aperture of the microscope objective, which results in 170 nm for green fluorescence and NA = 1.4. In contrast, precision measures the accuracy of determining the location of a single spot observed through the microscope. This was calculated to be (30) $d_{SPT} = \sqrt{(s^2 + a^2/12)/N}$, where s is the confocal resolution, a is the voxel dimension, and N is the total number of photons measured in the whole spot. This equation neglects shot noise, but for a rather large number of photons (500 and more), it can be neglected. For our confocal measurement with N∼500, we obtained a precision that is higher than 10 nm. The use of precision for improving the resolution, as described above, is being applied within the photoactivated localization microscopy and stochastic optical reconstruction microscopy super-resolution methods as well.

We calculated the loci mean-square displacements (MSDs) using the Imaris (Bitplane, CT) image analysis software package for locating coordinates of labeled genomic loci as well as a MATLAB (The MathWorks, Natick, MA) program that we developed for eliminating the rotational and translational drift of each nucleus. We then calculated the MSDs and the diffusion pattern and estimated the effective spring coefficient of each spot in two dimensions.

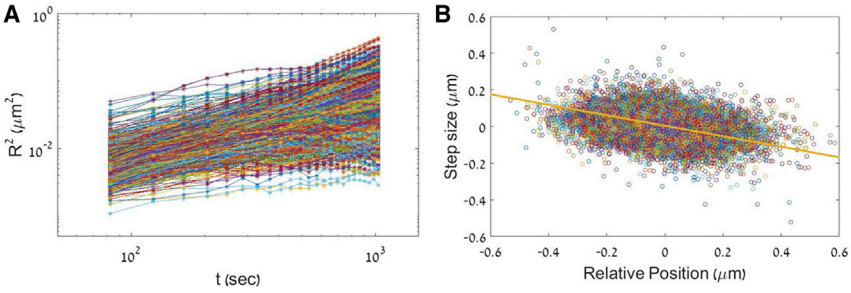

FIGURE 2 Dynamics of telomeres. (*A*) The MSD of all telomere trajectories in MEF cells (N = 1131) is given. (*B*) A scatter plot of step size versus the relative position (relative to the center of motion) is shown. The data were fitted to a linear curve (the *orange line*). Note that the fit may look biased, but this results from the tendency to follow the ellipse's main axis, which differs from the fit. An example is shown in Fig. S1. To see this figure in color, go online.

Analysis of the spring constant

To determine the elastic properties of single telomeres, we adopted a viscoelastic model formulated by the Langevin equation:

$$m\ddot{x} = -\gamma\dot{x} - k(x-\overline{x}) + f, \tag{1}$$

where γ is the friction coefficient, k is the spring constant, and f is a random external force assumed to have a zero average, $\langle f\rangle = 0$. The acceleration term can be neglected, assuming overdamping, which results from the low Reynolds number, which gives

$$\gamma\dot{x} = -k(x-\overline{x}) \tag{2}$$

Using the Einstein-Smoluchowski relation, γ can be expressed using the diffusion coefficient and the thermal energy k_BT:

$$\gamma = \frac{k_BT}{D}, \tag{3}$$

where k_B is the Boltzmann constant, T is the temperature, and D is the diffusion coefficient. Because the measurement is quantized, we can express the equation using the single-step position vectors measured at time differences dt:

$$\frac{k_BT}{D} \times \frac{(x_{i+1}-x_i)}{dt} = -k(x_i-\overline{x}) \tag{4}$$

This finally gives

$$k = -\frac{k_BT}{D} \times \frac{(x_{i+1}-x_i)}{dt(x_i-\overline{x})} \tag{5}$$

The diffusion coefficient, D, is calculated separately for each gene locus that we followed by taking only the short time intervals $\Delta t = 1$ (20.5 s) and $\Delta t = 2$ (41 s). During this short time interval, the diffusion is assumed to be normal and $\langle \Delta x^2\rangle = 4D\Delta t$. By rearranging Eq. 5, we obtained

$$\underbrace{x_{i+1}-x_i}_{Y} \approx \underbrace{-(Ddt/k_BT)k}_{a} \times \underbrace{(x_i-\overline{x})}_{X} \tag{6}$$

and plotted a scatter plot of the step sizes versus the position with respect to the average position (Fig. 2 *B*). Finally, the effective spring coefficient is extracted by fitting the scatter plot to a linear curve and finding a.

The linear fit with a negative slope resembles the first-order approximation for the potential well experienced by the particle. The farther it is from its central (average) position, the larger the force acting on it and the larger the step backward should be.

Assuming that the chromatin is isotropic, the force constant of each monomer is computed from all time steps N and all spatial dimensions d. Another method for estimating the effective spring coefficient is given by

$$k \approx -\frac{1}{d(N-1)} \sum_{i=1}^{d} \sum_{h=1}^{N-1} \frac{k_BT}{D} \times \frac{(x_{i+1}-x_i)}{dt(x_i-\overline{x})} \tag{7}$$

Both estimations were suggested and used before (26,27). Nevertheless, we found the first approach to be more accurate because with Eq. 7, small values of $\Delta x = x_i - \overline{x}$ contribute very large values that dominate the calculation because this is where the particles spend most of their time. Therefore, this method leads to erroneous values that over-emphasize k (30).

In contrast, by fitting a curve to the scatter plot found through Eq. 6, only the average value is taken into account in the fit for each Δx value.

RESULTS

Calculation of the force constant of chromatin loci

We measured the trajectories of different gene loci in MEF cells, calculated their MSDs in the xy plane (Fig. 2 *A*), plotted a scatter plot of the step sizes versus their relative position (Fig. 2 *B*), and estimated the effective spring coefficient of each locus (Fig. 3).

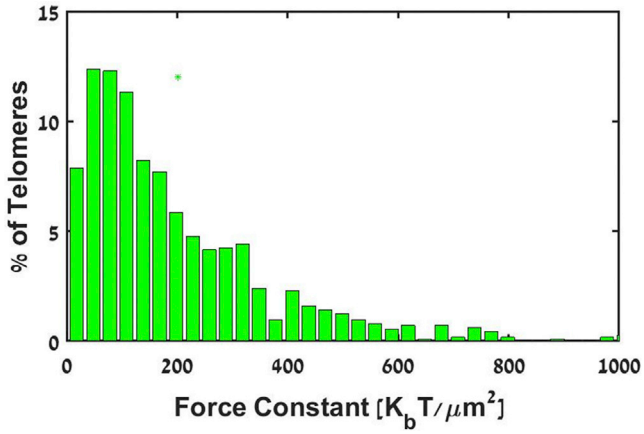

FIGURE 3 Effective spring constant distribution. The histogram presents the effective spring constant, which is obtained by a linear fit of the scatter plot (Eq. 6). It is based on an analysis of 1131 telomeres. To see this figure in color, go online.

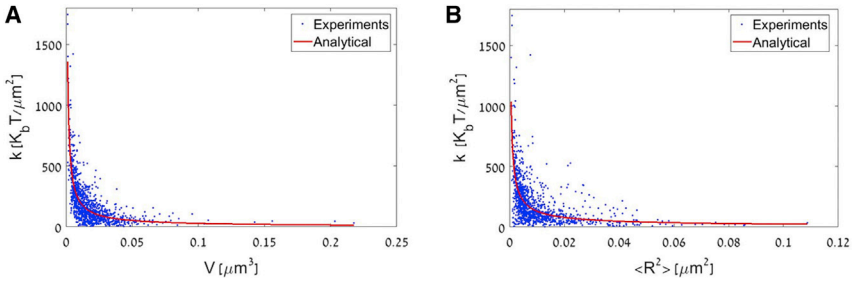

FIGURE 4 The motion of chromatin. (*A*) A scatter plot of the effective spring coefficient versus the volume of movement of all telomere trajectories (the *blue dots*) is given. The data were fitted to a power law, $k = av^{-b}$, with $a = 3.75 \pm 0.73$ [$k_BT \cdot \mu$m] and $b = 0.88 \pm 0.036$ (the *red line*). (*B*) A scatter plot of the effective spring coefficient versus the variance of the telomere trajectories (the *blue dots*) is shown. The data were fitted to a power law, $k = a\langle R^2\rangle^{-b}$, with $a = 4.66 \pm 1.3$ [$k_BT \cdot \mu$m] and $b = 0.725 \pm 0.047$ (the *red line*). The data included 1131 telomeres. To see this figure in color, go online.

Fig. 3 presents a histogram of the effective spring constants of all telomeres obtained by a linear fit of the data (Eq. 6). We found an average k-value of 202.2 [k_BT/μm^2], where 50% of the data are between 74.4 and 273.3 [k_BT/μm^2] (first-third quartiles). A comparison with the effective spring constants obtained by calculating with Eq. 7 is shown in Fig. S2.

To verify that the motion of the chromatin locus is indeed influenced by the polymer interactions, we present in Fig. 4 the effective spring coefficient versus the volume of movement, the volume that the telomere scanned during the measurement time of ~20 min, and the variance of the locus trajectory, calculated by

$$\langle R^2 \rangle = \frac{1}{N}\sum_{h=1}^{N}\left(R(h\Delta t) - \langle R\rangle\right)^2 \qquad (8)$$

The power-law decay of the graph is reasonable; when the spring coefficient is small, we expect the trajectory variance to be large and vice versa. We fitted the data to the expected polymer-like behavior found by Amitai et al. (25), $k = a/v^b$ and $k = a/\langle R^2\rangle^b$ and determined the a and b coefficients (Fig. 4). They differ from the predicted values, which were calculated to be $a = 2$ and $b = 1$ for a polymer model ((26), Eq. 12). This calculation is based on assumptions that do not take into account other features of the chromatin model, such as cross-links, that can alter the values. The same holds for the volume of movement. This suggests that the motion of the chromatin is localized because of a restoring harmonic force that originates from the polymer nature of the chromatin as well as other physical constraints. These may include the cross-links enforced by lamin A, which transforms the chromatin to a gel-like structure, and lamina that can bind chromatin close to the nuclear envelope. The same data is shown in a log-log scale in Fig. S3. It also emphasizes the relation between the spring coefficient and the trajectory variance or the volume of movement as described above.

A similar measurement and analysis were performed on centromeres, which are mostly located inside the chromosomes. It is well known that the centromeric area is normally more condensed with respect to the other chromosome parts because of its structure (32). We compared the effective spring coefficients of 1021 telomeres and 1040 centromeres in U2OS cells (Fig. 5) and found an average k-value of 147.62 [k_BT/μm^2] for telomeres, where 50% of the data are between 63.7 and 190.7 [k_BT/μm^2] (first-third quartiles), and 344.6 [k_BT/μm^2] for centromeres, where 50% of the data are between 170.3 and 472.1 [k_BT/μm^2] (first-third quartiles). A Student's t-test yielded a p-value of $p < 10^{-100}$, which confirms the significant difference between them. This result is in agreement with the differences we found in determining the dynamics of these different loci, where the diffusion of telomeres was found to be higher than that of centromeres (2).

The effect of different proteins on the effective force constant

In previous studies, we predicted that the chromatin is stabilized by cross-links of DNA, which transform the chromatin from a freely moving polymer to a gel-like structure; we

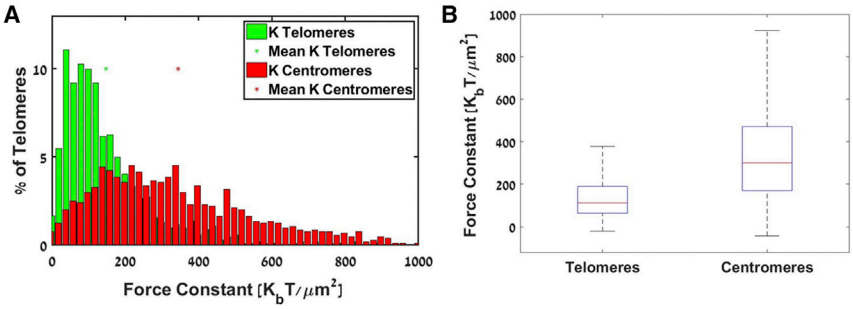

FIGURE 5 A comparison between the effective spring coefficient of telomeres and centromeres in U2OS cells. (*A*) Histograms are given of the effective spring constant, which was obtained by a linear fit of the scatter plot, as explained in Eq. 6, in telomeres (*green*) and in centromeres (*red*). (*B*) A boxplot of the two is shown. The data included 1021 telomeres and 1040 centromeres. A Student's t-test yielded a p-value of $p < 10^{-100}$. To see this figure in color, go online.

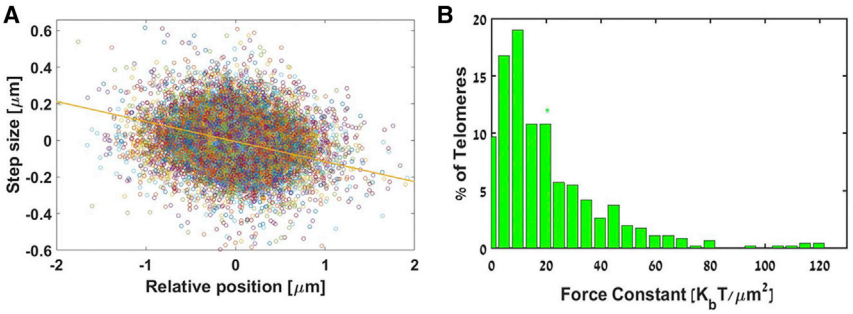

FIGURE 6 The effective spring constant of all telomeres in cells that do not express lamin A. (*A*) A scatter plot of step size versus the relative position (relative to the center of motion) of telomeres is given. The data were fitted with a linear fit (the *orange line*). (*B*) The histogram presents the effective spring constant, which was obtained by a linear fit of the scatter plot (Eq. 6). The data included 453 telomeres. To see this figure in color, go online.

found that lamin A has a major effect on chromatin dynamics (2,29). To test the effect of lamin A and other proteins on the mechanistic model that we propose here, we performed comparison measurements of the force constants in control cells and cells that are depleted of one protein at a time.

The effect of lamin A was tested in MEF cells that do not express lamin A protein in comparison to WT MEF cells. As before, we measured the dynamics of telomeres in these cells, plotted a scatter plot of the distribution of step sizes versus the relative spot position, and calculated the effective spring constant, as well as its distribution for all telomeres (Fig. 6). We found an average k-value of 20.47 [$k_BT/\mu m^2$], where 50% of the data are between 6.6 and 27.6 [$k_BT/\mu m^2$] (first-third quartiles).

Fig. S4 presents the effective spring coefficient versus the volume of movement and the variance of the locus trajectory (as explained before) in cells that do not express lamin A.

A comparison between the spring coefficient of WT cells and cells that do not express lamin A reveals a significant 10-fold reduction in the force constant, which indicates a dramatic change in the elasticity and confinement of the chromatin (Fig. 7). This dramatic reduction in the force constant implicates the increment of the chromatin dynamics in cells depleted of lamin A with respect to WT cells (2).

Next, we compared the effective spring coefficients that we obtained after the depletion of seven more proteins. First, we measured the trajectories of different spots in MEF cells that are depleted of a specific protein and calculated the effective spring coefficient. Each result was compared to WT MEF control cells. The comparison is shown in Fig. 8. As one can see, lamin A protein stands out as having a dramatic effect on the elastic properties of chromatin. The depletion of other proteins, such as BAF and lamin B1, also leads to a small decrease in the elastic constant, whereas others, such as cohesin and condensin, do not have any effect on the elastic properties of the chromatin.

Fig. 9 summarizes the results of the average effective spring coefficient that we obtained in WT MEF cells and MEF cells that are depleted of each specific protein that we tested. The table also shows the previous results of the volumes of motion and the anomalous exponent that we measured in those cells (29). We determined whether the effect is significant using a t-test between WT and knock-out (KO) cells and denoted in Fig. 9 a significant increase or decrease in blue or red, respectively.

Force coefficient as a function of the locus position

Finally, to test the effect of lamina and compare the chromatin dynamics close to the nuclear envelope and the nucleus interior, we compared the effective spring coefficient of spots inside the nucleus and spots that are closer to the nucleus envelope (Fig. 10). The separation between the spots was based on the convex hull, which defines the minimal area that confines all the spots. The spots that do not touch the convex hull are defined as the interior spots,

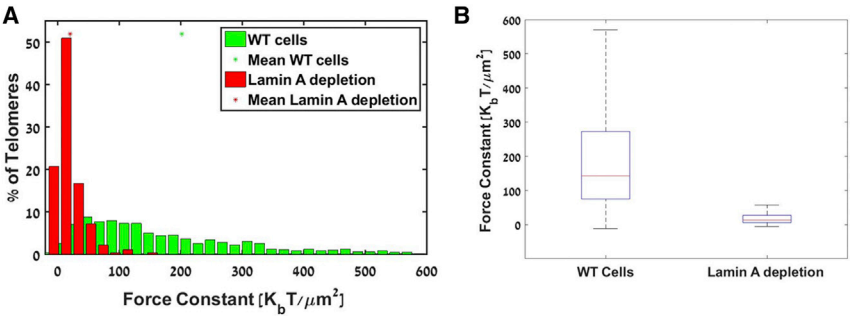

FIGURE 7 A comparison between the effective spring coefficient of WT cells and cells that do not express lamin A. (*A*) Histograms are given of the effective spring constant, which was obtained by a linear fit of the scatter plot, as explained in Eq. 6, in WT cells (*green*) and in cells that do not express lamin A (*red*). (*B*) A boxplot of the two is shown. The WT cells included 1131 telomeres, and the lamin A depletion cells included 453 telomeres. To see this figure in color, go online.

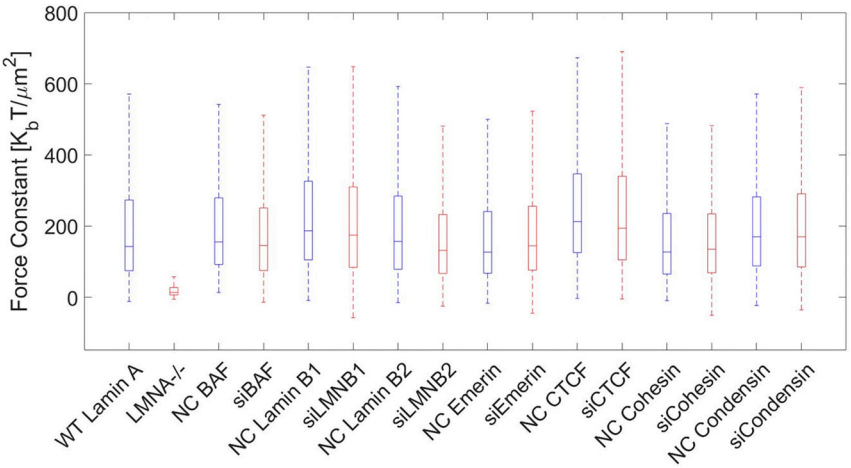

FIGURE 8 A comparison between the effective spring coefficient of WT cells and cells that do not express a specific protein. A boxplot of the effective spring constant of WT cells or negative control cells (NCs) and cells that are depleted of a specific protein is given. To see this figure in color, go online.

whereas the rest are defined as peripheral spots. We repeated the analysis in cells that do not express lamin A protein (Fig. 11).

In WT cells, no significant difference exists in the effective spring coefficient found for chromatin loci that are either inside the nucleus or located closer to the nuclear envelope. In cells that do not express lamin A, however, the effective spring coefficient inside the nucleus is somewhat larger than that of chromatin loci that are closer to the nuclear envelope.

Our previous works on chromosomes dynamics showed similar results (2,22). In normal cells, there is no significant difference between the volume of motion inside the nucleus and closer to the envelope. In contrast, in cells that do not express lamin A, the volume of movement inside the nucleus is smaller than the motion of chromatin sites that are closer to the nuclear envelope. Therefore, the spring coefficient is larger in the inner nucleus.

DISCUSSION

In this work, our aim was to study the elastic properties of chromatin in vivo. We focused on the elastic properties of several loci in the chromosomes and modeled their viscoelastic properties according to the Langevin equation and an approximation of the harmonic potential well experienced by each chromatin locus. Accordingly, we estimated the effective spring coefficient of each chromatin site, including telomeres and centromeres. We found that the average effective spring coefficient of telomeres in normal cells is 202.2 [$k_BT/\mu m^2$], and it is 344.6 [$k_BT/\mu m^2$] for centromeres. The effective spring coefficient that we found is larger than the value found previously in yeast chromatin sites (26); this indicates the stiffer elastic properties of chromatin in mammalian cells.

We then studied the effect of a series of proteins on the elastic properties of chromatin. We found that lamin A dramatically influences the elastic properties of chromatin

	WT cells / Negative Control			KO cell / si-RNA		
	<V> [μm^3]	<α>	<Kc> $\left[\frac{K_BT}{\mu m^2}\right]$	<V> [μm^3]	<α>	<Kc> $\left[\frac{K_BT}{\mu m^2}\right]$
Lamin A	0.02	0.50	202.20	0.20	1.00	20.47
BAF	0.02	0.50	244.60	0.03	0.65	194.87
Lamin B1	0.02	0.60	251.17	0.03	0.70	233.83
Emerin	0.03	0.81	182.96	0.03	0.74	196.32
CTCF	0.02	0.59	260.45	0.02	0.65	249.88
Cohesin	0.03	0.78	179.88	0.03	0.71	176.32
Lamin B2	0.02	0.73	205.45	0.03	0.71	174.46
Condensin	0.02	0.72	212.31	0.02	0.71	218.33

FIGURE 9 The dynamics and elastic results of WT cells and cells depleted of a specific protein. It shows the effective spring coefficient, the volume of motion, and the anomalous exponent that we measured and calculated for each cell. A significant effect, increase or decrease, between WT and KO cells is denoted in blue or red, respectively. To see this figure in color, go online.

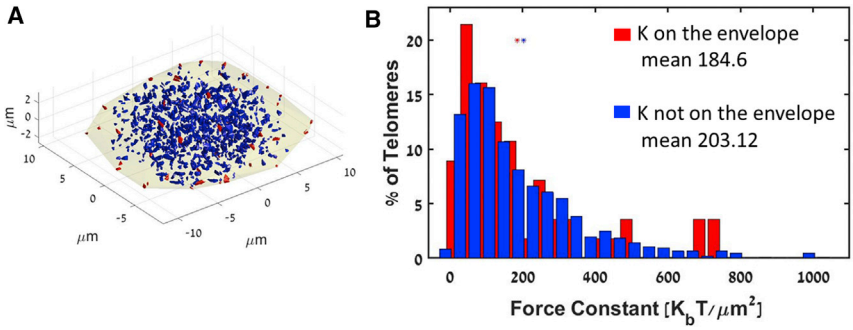

FIGURE 10 The effective spring coefficient as a function of the nucleus location in WT cells. (*A*) All the data we measured are presented together (1131 telomeres). The inner spots are presented in blue, and the spots that are closer to the envelope are presented in red. (*B*) Histograms of the effective spring constant in inner telomeres (*blue*) and in telomeres that are closer to the envelope (*red*) are given. To see this figure in color, go online.

and that the effective spring coefficient of chromatin sites in cells that did not express lamin A is only 20.47 [$k_BT/\mu m^2$], a reduction of ~90% with respect to WT cells. Other proteins that we measured did not significantly influence the elastic properties of the chromatin. These results are in agreement with our previous results, in which we measured the chromatin locus dynamics and the diffusion pattern (29).

Another study investigated the mechanical properties of chromatin and lamin A and found different mechanical response properties (33). Micromanipulation methods were used to isolate and stretch individual cell nuclei. It was found that chromatin maintains the nuclear morphology and resists small deformations, which determines the short-extension force response, whereas depletion of lamin A/C does not contribute significantly to this regime. The chromatin governs the response to small extensions and modulates the stiffness through the euchromatin and heterochromatin levels. In contrast, lamin A controls the strain stiffening at large extensions (33).

The viscoelastic properties of chromatin were also measured by analyzing the long-distance coherence of histone dynamics in HeLa cells (34). Coherence was detected based on the range of micrometers, beyond the typical size of a chromosome territory, and it was also explained through the elastic properties of chromatin. If the chromatin has significant elasticity, it can transmit local forces across large distances, even beyond the size of a chromosome territory, which would lead to coherent motions of large areas of the chromatin. It was also studied theoretically, showing the time-space correlations of chromatin loci (35). Here, a coarse-grain model of chromatin was assumed, in which each two monomer segments are connected by springs, together with a hydrodynamic drag in the nucleoplasm. This emphasizes the importance of the elasticity of the polymer, together with the viscoelastic properties of the nucleoplasm.

We also found that in normal cells, the effective spring coefficient was not affected by its position inside the nucleus. Different results, however, were found in yeast cells, where it was found that when the observed monomer is closer to the anchoring locus, the trajectory is more localized, and the effective spring constant is larger (26). This difference can be explained because yeast cells are much smaller and are known to anchor chromosomes tightly to the nuclear envelope.

In cells that do not express lamin A, the effective spring coefficient is somewhat larger for sites inside the nucleus relative to sites that are close to the nuclear envelope. These results are also in agreement with our dynamics results (2,22). This suggests that although lamina interacts with chromatin on the nuclear envelope, the inner nuclear structure of chromatin with the lamin A cross-links provides stiffer elastic properties in the nuclear volume.

The force coefficient was found to be distributed differently in WT cells versus cells that are depleted of lamin A. In WT cells, the coefficient has a rather broad distribution, whereas in lamin A-depleted cells, the coefficient

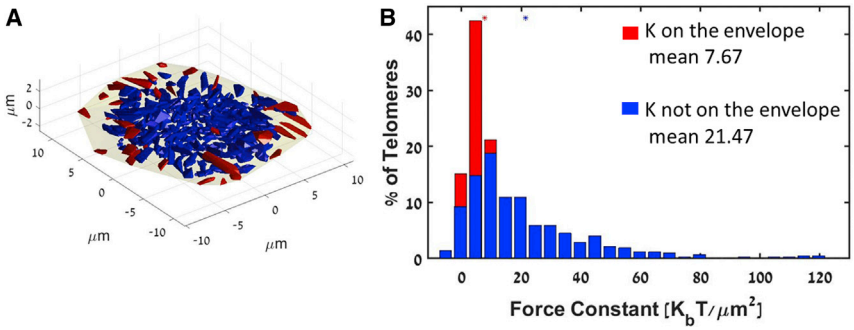

FIGURE 11 The effective spring coefficient as a function of the position of the chromatin loci in the nucleus in cells that do not express lamin A. (*A*) The volume of motion of 453 telomeres is shown; the inner spots are denoted in blue, and spots that are closer to the envelope are denoted in red. (*B*) Histograms of the effective spring constant in inner telomeres (*blue*) and in telomeres closer to the envelope (*red*) are given. To see this figure in color, go online.

average is ~10-fold smaller, and the distribution is much narrower. These findings indicate that the local environment in WT cells is heterogeneous, perhaps because of a different local condensation of the chromatin, eu-, and heterochromatin. The fact that lamin A depletion reduces the force constant and makes the distribution narrower can be explained by the effect of the loss of cross-links in the entire nuclear volume and the anchoring to the lamina.

All together, we confirmed that the elastic properties of chromatin can be extracted from single chromatin sites. The force constant is larger in the inner nuclear volume than in the envelope in lamin A depletion cells, and it is strongly dominated by lamin A, whereas other proteins have no significant or only a small effect. This strongly supports the notion that chromatin properties resemble those of a polymer gel rather than a simpler Rouse model or a fractal-like structure. These elastic properties significantly affect many of the nuclear functions and should be further studied.

Furthermore, a connection between the mechanical properties of the cell nucleus and cancer metastasis is emerging lately. The nucleus, which is the largest cellular organelle, is rather stiff in normal cells, but once it becomes less elastic, as we found, it can be deformed more easily and stops acting as an obstacle when the cell metastasizes through narrow capillaries (36,37).

SUPPORTING MATERIAL

Supporting Material can be found online at https://doi.org/10.1016/j.bpj.2020.04.002.

AUTHOR CONTRIBUTIONS

This stuy was designed by A.V. and Y.G., who provided conceptual and technical guidance for the project. A.V. performed the measurements, planned the analytical tools, and analyzed the data. I.B. contributed to the measurements and to the design of the project. The manuscript was written by A.V. and Y.G. I.B. provided useful comments.

ACKNOWLEDGMENTS

We thank A. Amitai (Massachusetts Institute of Technology) for fruitful guidance and discussion.

The authors would like to acknowledge financial support from the Israel Science Foundation grants 1902/12 and 1219/17, the Ministry of Science, Technology and Space grant 3-13733, and from the S. Grosskopf grant for "Generalized dynamic measurements in live cells."

REFERENCES

1. Pombo, A., and N. Dillon. 2015. Three-dimensional genome architecture: players and mechanisms. *Nat. Rev. Mol. Cell Biol.* 16:245–257.
2. Bronshtein, I., E. Kepten, …, Y. Garini. 2015. Loss of lamin A function increases chromatin dynamics in the nuclear interior. *Nat. Commun.* 6:8044.
3. Ho, C. Y., and J. Lammerding. 2012. Lamins at a glance. *J. Cell Sci.* 125:2087–2093.
4. van Steensel, B., and A. S. Belmont. 2017. Lamina-associated domains: links with chromosome architecture, heterochromatin, and gene repression. *Cell.* 169:780–791.
5. Moir, R. D., M. Yoon, …, R. D. Goldman. 2000. Nuclear lamins A and B1: different pathways of assembly during nuclear envelope formation in living cells. *J. Cell Biol.* 151:1155–1168.
6. Broers, J. L., B. M. Machiels, …, F. C. Ramaekers. 1999. Dynamics of the nuclear lamina as monitored by GFP-tagged A-type lamins. *J. Cell Sci.* 112:3463–3475.
7. Bustin, M., and T. Misteli. 2016. Nongenetic functions of the genome. *Science.* 352:aad6933.
8. Maeshima, K., S. Tamura, and Y. Shimamoto. 2018. Chromatin as a nuclear spring. *Biophys. Physicobiol.* 15:189–195.
9. Cremer, T., and C. Cremer. 2001. Chromosome territories, nuclear architecture and gene regulation in mammalian cells. *Nat. Rev. Genet.* 2:292–301.
10. Cremer, T., and M. Cremer. 2010. Chromosome territories. *Cold Spring Harb. Perspect. Biol.* 2:a003889.
11. Shivashankar, G. V. 2019. Mechanical regulation of genome architecture and cell-fate decisions. *Curr. Opin. Cell Biol.* 56:115–121.
12. Rubinstein, M., and R. H. Colby. 2003. Polymer Physics. Oxford University Press, Oxford, UK.
13. Lu, Y., B. Weers, and N. C. Stellwagen. 2001–2002. DNA persistence length revisited. *Biopolymers.* 61:261–275.
14. Lindner, M., G. Nir, …, Y. Garini. 2013. Dynamic analysis of a diffusing particle in a trapping potential. *Phys. Rev. E Stat. Nonlin. Soft Matter Phys.* 87:022716.
15. Roth, E., A. Glick Azaria, …, Y. Garini. 2018. Measuring the conformation and persistence length of single-stranded DNA using a DNA origami structure. *Nano Lett.* 18:6703–6709.
16. Doi, M., and S. F. Edwards. 1988. The Theory of Polymer Dynamics. Clarendon Press, Oxford, UK.
17. Osmanović, D., and Y. Rabin. 2017. Dynamics of active Rouse chains. *Soft Matter.* 13:963–968.
18. Cui, Y., and C. Bustamante. 2000. Pulling a single chromatin fiber reveals the forces that maintain its higher-order structure. *Proc. Natl. Acad. Sci. USA.* 97:127–132.
19. Dekker, J., K. Rippe, …, N. Kleckner. 2002. Capturing chromosome conformation. *Science.* 295:1306–1311.
20. Buckle, A., C. A. Brackley, …, N. Gilbert. 2018. Polymer simulations of heteromorphic chromatin predict the 3d folding of complex genomic loci. *Mol. Cell.* 72:786–797.e11.
21. Bloom, K. S. 2008. Beyond the code: the mechanical properties of DNA as they relate to mitosis. *Chromosoma.* 117:103–110.
22. Vivante, A., E. Brozgol, …, Y. Garini. 2017. Genome organization in the nucleus: from dynamic measurements to a functional model. *Methods.* 123:128–137.
23. Bronstein, I., Y. Israel, …, Y. Garini. 2009. Transient anomalous diffusion of telomeres in the nucleus of mammalian cells. *Phys. Rev. Lett.* 103:018102.
24. Kepten, E., I. Bronshtein, and Y. Garini. 2011. Ergodicity convergence test suggests telomere motion obeys fractional dynamics. *Phys. Rev. E Stat. Nonlin. Soft Matter Phys.* 83:041919.
25. Kepten, E., I. Bronshtein, and Y. Garini. 2013. Improved estimation of anomalous diffusion exponents in single-particle tracking experiments. *Phys. Rev. E Stat. Nonlin. Soft Matter Phys.* 87:052713.
26. Amitai, A., M. Toulouze, …, D. Holcman. 2015. Analysis of single locus trajectories for extracting in vivo chromatin tethering interactions. *PLoS Comput. Biol.* 11:e1004433.
27. Amitai, A., A. Seeber, …, D. Holcman. 2017. Visualization of chromatin decompaction and break site extrusion as predicted by statistical polymer modeling of single-locus trajectories. *Cell Rep.* 18:1200–1214.

28. Polovnikov, K. E., M. Gherardi, …, M. V. Tamm. 2018. Fractal folding and medium viscoelasticity contribute jointly to chromosome dynamics. *Phys. Rev. Lett.* 120:088101.

29. Vivante, A., E. Brozgol, …, Y. Garini. 2019. Chromatin dynamics governed by a set of nuclear structural proteins. *Genes Chromosomes Cancer.* 58:437–451.

30. Shukron, O., A. Seeber, …, D. Holcman. 2019. Advances using single-particle trajectories to reconstruct chromatin organization and dynamics. *Trends Genet.* 35:685–705.

31. Thompson, R. E., D. R. Larson, and W. W. Webb. 2002. Precise nanometer localization analysis for individual fluorescent probes. *Biophys. J.* 82:2775–2783.

32. Gilbert, N., and J. Allan. 2001. Distinctive higher-order chromatin structure at mammalian centromeres. *Proc. Natl. Acad. Sci. USA.* 98:11949–11954.

33. Stephens, A. D., E. J. Banigan, …, J. F. Marko. 2017. Chromatin and lamin A determine two different mechanical response regimes of the cell nucleus. *Mol. Biol. Cell.* 28:1984–1996.

34. Zidovska, A., D. A. Weitz, and T. J. Mitchison. 2013. Micron-scale coherence in interphase chromatin dynamics. *Proc. Natl. Acad. Sci. USA.* 110:15555–15560.

35. Lampo, T. J., A. S. Kennard, and A. J. Spakowitz. 2016. Physical modeling of dynamic coupling between chromosomal loci. *Biophys. J.* 110:338–347.

36. Denais, C., and J. Lammerding. 2014. Nuclear mechanics in cancer. *Adv. Exp. Med. Biol.* 773:435–470.

37. Contu, F., A. Rangel-Pozzo, …, S. Mai. 2018. Distinct 3D structural patterns of lamin A/C expression in Hodgkin and Reed-Sternberg cells. *Cancers (Basel).* 10:E286.